A time averaged semiclassical approach to IR spectroscopy

Cecilia Lanzi, Chiara Aieta, Michele Ceotto,* and Riccardo Conte†

Dipartimento di Chimica, Università degli Studi di Milano,

via Golgi 19, 20133 Milano, Italy

Abstract

We propose a new semiclassical approach to the calculation of molecular IR spectra. The method employs Kaledin and Miller's time averaging technique upon symmetrization of the quantum dipole-dipole autocorrelation function. Spectra at high and low temperature are investigated. In the first case we are able to point out the possible presence of hot bands in the molecular absorption lineshape. In the second case we are able to reproduce accurate IR spectra as demonstrated by a calculation of the IR spectrum of the water molecule, which is within 4% of the exact intensity. Our time averaged IR spectra can be directly compared to time averaged semiclassical power spectra as shown in an application to the CO_2 molecule, which points out the differences between IR and power spectra and demonstrates that our new approach can identify active IR transitions correctly. Overall the method features excellent accuracy in calculating absorption intensities and provides estimates for the frequencies of vibrations in agreement with the corresponding power spectra. In perspective this work opens up the possibility to interface the new method with the semiclassical techniques developed for power spectra, such as the divide-and-conquer one, to get accurate IR spectra of complex and high dimensional molecular systems.

*Electronic address: michele.ceotto@unimi.it

†Electronic address: riccardo.conte1@unimi.it

I. INTRODUCTION

Infrared (IR) spectroscopy is a widely used technique in chemistry, often employed for pivotal goals like characterization of synthesis intermediates, investigation of molecular interactions and structure, evaluation of the degree of polymerization, quantitative measurement of molecular concentrations, and improvement of the recycling process.[1–3] However, an experimental IR spectrum is characterized by a large number of features due to fundamental transitions, overtones, and combination bands, which are often close to each other in energy and difficult to identify. Furthermore, the complexity of the spectrum rapidly increases with the dimensionality of the system, making it harder and harder to experimentally assign every single feature to specific vibrational molecular motions.

The main goal of a theoretical approach to IR spectroscopy is to reproduce experimental spectra adding some physical insights. These include (but are not limited to) characterization of the observed spectral transitions in terms of decomposition of the signal on simple basic molecular motions,[4, 5] ability to discern between signals lying close to each other, determination of relaxation processes based on the calculated absorption lineshape,[6] possibility to study localized interactions between a molecule and its environment in solvated systems.[7]

From a theoretical point of view, the molecular IR spectrum (here and usually indicated as $\alpha(\omega, T)$) describes the interaction (i.e. absorption or stimulated emission of energy) between a molecule and an incoming time-dependent electric field (E) under the form of a pulse or a periodic field in the IR range of frequencies (ω). The IR range of frequencies is commonly divided into the far-, mid-, or near- infrared regions according to their wavelengths compared to the visible radiation. Molecular vibrations typically involve the 400-4000 cm^{-1} region, which is the mid-infrared one.

The IR spectrum $\alpha(\omega, T)$ can be theoretically obtained either from first order time-dependent perturbation theory as a sum over states expression involving transition dipole moments, or as the Fourier transform of a quantum dipole-dipole autocorrelation function.[8] Another possible approach consists in looking at the time dependence of the initial state population under the radiation field E, which leads to link $\alpha(\omega, T)$ to the imaginary part of the Fourier transform of the instantaneous

dipole displacement (i.e. fluctuation) from equilibrium.[9] Temperature is included by means of the Boltzmann probability of populating the initial and final states involved in the vibrational transitions. It influences the intensity of absorption, which is related to the difference in population between the two involved vibrational states, but it does not affect the energy (i.e. frequency) of the transition.

Several theoretical methods have been developed to calculate quantum mechanically IR spectra, involving both time-independent and time-dependent approaches.[10–18] In this manuscript we focus on a specific type of time-dependent approach known as the semiclassical (SC) dynamics approach.[19–21] Semiclassical dynamics is a quite general approach, which has been employed in a variety of problems other than spectroscopy, including, for instance, kinetics,[22–28] wavefunction determination,[29, 30] and dissipative dynamics,[31–33] where it can be cast in a mixed quantum-classical framework.[34–39] When dealing with spectroscopy, the main goal of SC dynamics is to get quantum effects at an affordable computational cost starting from classical trajectories evolved under the molecular Hamiltonian.[34, 40–46] The flexibility of the SC approach to spectroscopy is evident: being based on classical trajectories it is amenable to be applied to large molecular systems; it can be interfaced to *ab initio* molecular dynamics; it provides a way to connect spectroscopic signals directly to molecular motions; being a time-dependent approach it can account for relaxation processes. However, several issues needed to be overcome over the years before making SC spectroscopy doable in practice.

The theory of SC spectroscopy has been mainly developed for power spectra, i.e. spectra obtained upon Fourier transforming the survival amplitude of a reference and arbitrary wavepacket. In this way it is possible to determine all the energy levels of the system and, by difference, the frequencies related to the corresponding transitions. The first issue to be solved concerned the convergence of the semiclassical calculation. This is what encouraged development of the time average technique. By applying a time average to the SC propagator, Kaledin and Miller showed that it is possible to come up with a positive-definite integrand and a much easier and faster convergence of results.[47, 48] Their technique is known as the Time Averaged Semiclassical Initial Value Representation (TA SCIVR). In spite of the advance in-

troduced by TA SCIVR, SC vibrational spectroscopy was still far from the possibility to be employed with *ab initio* molecular dynamics, a fundamental step to have the method applicable to large molecular systems. This goal was reached by one of us with the Multiple Coherent Semiclassical Initial Value Representation (MC SCIVR), based on a tailored choice of the reference state and trajectory energy.[49] At this point, a final problem was to be faced due to the progressive deterioration of the signal to noise ratio as the dimensionality of the system increases. This was solved by means of a divide-and-conquer technique successfully developed in our group.[50] The Divide-and-Conquer Semiclassical Initial Value Representation (DC SCIVR) allows one to deal with large dimensional systems by partitioning the full-dimensional vibrational space into smaller subspaces made of the modes more strongly coupled to each other. Interactions between modes belonging to different subspaces are still approximately taken into account thanks to the full-dimensional dynamics employed in the DC-SCIVR calculation. DC SCIVR has allowed us to study the vibrational spectroscopy of systems in solution, condensed phase, or adsorbed on solid surfaces.[7, 51–53] Very recently, accuracy and efficiency of SC vibrational spectroscopy have been increased by the development in our group of a technique able to improve the sampling of initial conditions for the semiclassical runs. This technique adopts an adiabatic switching procedure and is known as adiabatically switched semiclassical initial value representation (AS SCIVR).[54–56] It is worth noticing that a recent alternative and effective approach to calculate semiclassical power spectra is based on filter diagonalization of the survival amplitude. This method is based on very short trajectory evolution, it does not rely on time average, and it has been shown to be able to get reliable results on fitted potential energy surfaces.[57]

The advances described above have been undertaken for the calculation of power spectra. However, for comparison to experimental IR spectra both intensities and selection rules must be accurately reproduced by the calculation. On this regard, calculations of semiclassical vibronic spectra, which involve transitions at energies higher than those found in IR spectra, able to account for transition energies and intensities have been successfully performed in the Vanicek group by means of im-

proved SC thawed Gaussian techniques.[58–60] As for semiclassical IR spectroscopy, two methods have already been developed in our group. In one case, it is shown how to calculate SC wavefunctions starting from SC power spectra, and from there the IR spectrum is constructed.[61] In the second approach the lineshape of the power spectrum is the starting point to reconstruct the IR spectrum with the need to calculate only the ground state wavefunction for a fully anharmonic IR spectrum or no wavefunction at all if a semi-anharmonic IR spectrum is sufficient.[62] Both methods have been successfully applied to a few relevant molecular systems, but they generally are more elaborated and less user-friendly than an SC power spectrum calculation.

In this paper our goal is to introduce a new SC approach to IR spectroscopy showing how it is possible to take advantage of the time average technique to calculate IR spectra with computational cost and theoretical complexity similar to those of a power spectrum calculation. The paper is structured as follows: First we elaborate on our new semiclassical theory for IR spectra; then, we present applications to a model Morse oscillator and calculate IR spectra for the water molecule and the CO_2 molecule; eventually the paper ends with some comments and future perspectives.

II. THEORY

We start from the general definition of the IR spectrum of any isotropic and homogeneous molecular system, which is derived from the quantum first-order perturbation theory [8]

$$\alpha(\omega, T) \propto \sum_{i \neq f} \omega_{fi} \left[p_i(T) - p_f(T) \right] \left| \langle \Psi_i | \hat{\mu} | \Psi_f \rangle \right|^2 \delta(\omega_{fi} - \omega), \tag{1}$$

where the proportionality symbol means we avoid reporting some constant terms that cancel out when looking at the relative intensities of the molecular absorption peaks. Therefore these constant terms will be neglected from now on.

In Eq. 1 $p_i = e^{-\beta E_i}/Z$, with $\beta = (k_B T)^{-1}$ and $Z = \sum_n e^{-\beta E_n}$, represents the probability of occupying the vibrational eigenstate Ψ_i at temperature T. $\hat{\mu}$ is the transition dipole moment operator, and $\omega_{fi} = (E_f - E_i)/\hbar$ is the transition frequency corresponding to the difference between the eigenenergies of the vibrational states

involved in the transition. By exploiting the definition of p_i, one can separate $\alpha(\omega, T)$ into a product of terms, one of which describing the so-called absorption lineshape $\sigma(\omega, T)$. The transition frequencies appearing in the terms multiplying $\sigma(\omega, T)$ can be set equal to ω due to the Dirac delta that implies $\omega_{fi} = \omega$. In formulae

$$\alpha(\omega, T) = \omega(1 - e^{-\beta\hbar\omega})\sigma(\omega, T) \tag{2a}$$

$$\sigma(\omega, T) = \sum_{i \neq f} p_i(T) \left|\langle \Psi_i | \hat{\mu} | \Psi_f \rangle\right|^2 \delta(\omega_{fi} - \omega). \tag{2b}$$

The absorption lineshape can be also calculated as Fourier transform of the dipole-dipole quantum autocorrelation function $C_{\mu\mu}(t, T)$.

$$\sigma(\omega, T) = \frac{1}{2\pi} \int_{-\infty}^{+\infty} dt\, e^{-i\omega t} C_{\mu\mu}(t, T). \tag{3}$$

The expression of $C_{\mu\mu}(t, T)$, by making the quantum mechanical expression of the average over the density matrix explicit and considering the Heisenberg picture of the transition dipole moment operator at time t, $\hat{\mu}(t) = e^{i\hat{H}t/\hbar}\ \hat{\mu}\ e^{-i\hat{H}t/\hbar}$, is

$$C_{\mu\mu}(t, T) = \langle \hat{\mu}(0)\hat{\mu}(t) \rangle = \mathrm{Tr}\left[\hat{B}(\beta)\ \hat{\mu}\ e^{i\hat{H}t/\hbar}\ \hat{\mu}\ e^{-i\hat{H}t/\hbar}\right], \tag{4}$$

where $\hat{B}(\beta) = e^{-\beta\hat{H}}/Z$ is the Boltzmann operator and we have introduced the notation $\hat{\mu} = \hat{\mu}(0)$. At this point, in order to obtain a somehow symmetrized form of $C_{\mu\mu}(t, T)$,[63] we express the Boltzmann operator as the product of two $\hat{B}(\beta/2)$ terms; then, we perform a cyclic permutation within the trace elements and use the property of commutation between $\hat{B}(\beta/2)$ and the time evolution operator $e^{-i\hat{H}t/\hbar}$. In this way, we get

$$C_{\mu\mu}(t, T) = \mathrm{Tr}\left[\hat{B}(\beta/2)\ \hat{\mu}\ e^{i\hat{H}t/\hbar}\ \hat{\mu}\ \hat{B}(\beta/2)\ e^{-i\hat{H}t/\hbar}\right]. \tag{5}$$

We now move to the treatment of the time evolution operators in Eq. 5, which cannot be evaluated exactly for most real systems. In this work, we employ the Heller-Herman-Kluk-Kay (HHKK) approximation to the quantum propagator, of wide use in the field of semiclassical dynamics.[64–66] The HHKK propagator was originally developed by combining the initial value representation (IVR) proposed by Miller[43, 67–69] and the use of coherent state basis, as suggested by Heller.[66]

This semiclassical propagator, for a system consisting of N_v vibrational degrees of freedom, in fact, makes use of coherent states of the kind

$$\langle \boldsymbol{x}|\boldsymbol{p}_t\boldsymbol{Q}_t\rangle = \left(\frac{\det(\boldsymbol{\Gamma})}{\pi^{N_\nu}}\right)^{\frac{N_\nu}{4}} e^{-\frac{1}{2}(\boldsymbol{x}-\boldsymbol{Q}_t)^{\mathrm{T}}\boldsymbol{\Gamma}(\boldsymbol{x}-\boldsymbol{Q}_t)+\frac{i}{\hbar}\boldsymbol{p}_t^{\mathrm{T}}(\boldsymbol{x}-\boldsymbol{Q}_t)}, \tag{6}$$

where $\boldsymbol{p}_t$ and $\boldsymbol{Q}_t$ are the instantaneous linear momenta and normal mode displacements $\boldsymbol{Q}_t = \boldsymbol{q}_t - \boldsymbol{q}_{eq}$, respectively, and $\boldsymbol{\Gamma}$ is the matrix of the coherent state widths, which we choose to be diagonal with time-independent elements equal to the harmonic vibrational frequencies (ω_j) of the system.

The HHKK propagator reads as

$$e^{-\frac{i}{\hbar}\hat{H}t} \approx \left(\frac{1}{2\pi\hbar}\right)^{N_\nu} \iint d\boldsymbol{p}_0 d\boldsymbol{Q}_0\, C_t(\boldsymbol{p}_0,\boldsymbol{Q}_0) e^{iS_t(\boldsymbol{p}_0,\boldsymbol{Q}_0)/\hbar}\, |\boldsymbol{p}_t\boldsymbol{Q}_t\rangle\, \langle \boldsymbol{p}_0\boldsymbol{Q}_0|\,, \tag{7}$$

where $(\boldsymbol{p}_0,\boldsymbol{Q}_0)$ are the initial linear momenta and normal mode displacements which are evolved in time under the classical vibrational Hamiltonian $H(\boldsymbol{p},\boldsymbol{Q}) = \boldsymbol{p}^2/2m + V(\boldsymbol{Q})$, $S_t(\boldsymbol{p}_0,\boldsymbol{Q}_0)$ is the corresponding classical action evaluated at time t, and $C_t(\boldsymbol{p}_0,\boldsymbol{Q}_0)$ is the pre-exponential factor (indicated, as common practice in the field, with the same symbol (C) of the autocorrelation function above, but not to be confused with it)

$$C_t(\boldsymbol{p}_0,\boldsymbol{Q}_0) = \sqrt{\det\left[\frac{1}{2}\left(\mathbf{M}_{QQ} + \boldsymbol{\Gamma}^{-1}\mathbf{M}_{pp}\boldsymbol{\Gamma} - i\hbar\mathbf{M}_{Qp}\boldsymbol{\Gamma} + \frac{i}{\hbar}\boldsymbol{\Gamma}^{-1}\mathbf{M}_{pQ}\right)\right]}, \tag{8}$$

with $\mathbf{M}_{ij}$ being the elements of the monodromy (or stability) matrix, defined as $\mathbf{M}_{ij} = \frac{\partial \mathbf{i}_t}{\partial \mathbf{j}_0}$ ($\mathbf{i},\mathbf{j}$=$\mathbf{p},\mathbf{Q}$). Due to inaccuracies in the numerical integration which build up during the simulation, the magnitude of the determinant of the stability matrix elements (expected to be of constant value equal to 1 during the entire simulation) tends to increase with the chaoticity of the trajectories, leading to unphysical values of the pre-exponential factor. To avoid this issue, in this work we adopt a well-established procedure consisting in eliminating those chaotic trajectories for which the determinant of the monodromy matrix diverges from unity more than a fixed threshold.

One of the reasons why the HHKK formulation of the propagator was originally introduced is that it allows the use of Monte Carlo integration techniques to speed up the convergence of the multi-dimensional phase space integration. Nevertheless,

when dealing with systems having already a small number of degrees of freedom, the evolution of a high number of classical trajectories is required to reach convergence. Therefore, some filtering procedures are usually employed to further speed up convergence. In this work we make use of the time average (TA) technique developed by Kaledin and Miller,[47, 48] a well-known procedure which allows to rearrange the integrand of the phase-space average of Eq. 7 to make it positive-definite, hence much more easily integrable, with no loss in accuracy.

Indeed, starting from

$$C_{\mu\mu}(t,T) = \iint \frac{d\boldsymbol{p}_0 d\boldsymbol{Q}_0}{(2\pi\hbar)^{N_\nu}} \iint \frac{d\boldsymbol{p}'_0 d\boldsymbol{Q}'_0}{(2\pi\hbar)^{N_\nu}} C_t^*(\boldsymbol{p}_0,\boldsymbol{Q}_0) C_t(\boldsymbol{p}'_0,\boldsymbol{Q}'_0) e^{-iS_t(\boldsymbol{p}_0,\boldsymbol{Q}_0)/\hbar} \times e^{iS_t(\boldsymbol{p}'_0,\boldsymbol{Q}'_0)/\hbar} \langle \boldsymbol{p}'_0\boldsymbol{Q}'_0|\hat{B}(\beta/2)\hat{\mu}|\boldsymbol{p}_0\boldsymbol{Q}_0\rangle \langle \boldsymbol{p}_t\boldsymbol{Q}_t|\hat{\mu}\hat{B}(\beta/2)|\boldsymbol{p}'_t\boldsymbol{Q}'_t\rangle \,, \tag{9}$$

obtained by inserting Eq. 7 into Eq. 5 twice, following Kaledin and Miller, one can proceed by adding a time average based on the total simulation time T_s coming up with the following expression for the absorption lineshape

$$\sigma(\omega,T) = \iint \frac{d\boldsymbol{p}_0 d\boldsymbol{Q}_0}{(2\pi\hbar)^{N_\nu}} \iint \frac{d\boldsymbol{p}'_0 d\boldsymbol{Q}'_0}{(2\pi\hbar)^{N_\nu}} \frac{1}{T_s} \int_0^{T_s} dt_1 \, \frac{Re}{\pi} \int_0^{+\infty} dt \, e^{-i\omega t} \times C^*_{t+t_1}(\boldsymbol{p}_{t_1},\boldsymbol{Q}_{t_1}) C_{t+t_1}(\boldsymbol{p}'_{t_1},\boldsymbol{Q}'_{t_1}) e^{-iS_{t+t_1}(\boldsymbol{p}_{t_1},\boldsymbol{Q}_{t_1})/\hbar} e^{iS_{t+t_1}(\boldsymbol{p}'_{t_1},\boldsymbol{Q}'_{t_1})/\hbar} \times \langle \boldsymbol{p}'_{t_1}\boldsymbol{Q}'_{t_1}|\hat{B}(\beta/2)\hat{\mu}|\boldsymbol{p}_{t_1}\boldsymbol{Q}_{t_1}\rangle \langle \boldsymbol{p}_{t+t_1}\boldsymbol{Q}_{t+t_1}|\hat{\mu}\hat{B}(\beta/2)|\boldsymbol{p}'_{t+t_1}\boldsymbol{Q}'_{t+t_1}\rangle \,, \tag{10}$$

where $(\boldsymbol{p}_{t_1},\boldsymbol{Q}_{t_1})$ and $(\boldsymbol{p}_{t+t_1},\boldsymbol{Q}_{t+t_1})$ represent the momenta and displacements at time t_1 and $t+t_1$, respectively, evolving from the initial conditions $(\boldsymbol{p}_0,\boldsymbol{Q}_0)$, and analogously for $(\boldsymbol{p}'_{t_1},\boldsymbol{Q}'_{t_1})$ and $(\boldsymbol{p}'_{t+t_1},\boldsymbol{Q}'_{t+t_1})$, starting from $(\boldsymbol{p}'_0,\boldsymbol{Q}'_0)$. At this point, we can introduce the change in time variables $t_2 = t+t_1$, or $t = t_2 - t_1$ and consider that the action

$$S_{t+t_1}(\boldsymbol{p}_{t_1},\boldsymbol{Q}_{t_1}) = S_{t_2}(\boldsymbol{p}_{t_1},\boldsymbol{Q}_{t_1}) = \int_{t_1}^{t_2} dt' \mathcal{L}(t') \,, \tag{11}$$

with $\mathcal{L}$ being the Lagrangian $\boldsymbol{p}^2/2m - V(\boldsymbol{Q})$, can be recast as

$$\int_{t_1}^{t_2} dt' \mathcal{L}(t') \; = \int_0^{t_2} dt' \mathcal{L}(t') - \int_0^{t_1} dt' \mathcal{L}(t') = S_{t_2}(\boldsymbol{p}_0,\boldsymbol{Q}_0) - S_{t_1}(\boldsymbol{p}_0,\boldsymbol{Q}_0) \,. \tag{12}$$

The same stands for $S_{t+t_1}(\boldsymbol{p}'_{t_1},\boldsymbol{Q}'_{t_1})$, which is equal to $S_{t_2}(\boldsymbol{p}'_0,\boldsymbol{Q}'_0) - S_{t_1}(\boldsymbol{p}'_0,\boldsymbol{Q}'_0)$. Then, in order to further simplify the integrand of Eq. 10 and advance with the time

averaging procedure, we take advantage of the so-called separable approximation to the pre-exponential factors

$$C_{t_2}(\boldsymbol{p}_{t_1}, \boldsymbol{Q}_{t_1}) \approx e^{i\phi(t_2)/\hbar} e^{-i\phi(t_1)/\hbar}, \tag{13}$$

where $\phi(t) = \phi_t(\boldsymbol{p}_0, \boldsymbol{Q}_0)$ and it is calculated from its definition which is $\phi_t(\boldsymbol{p}_0, \boldsymbol{Q}_0) =$ phase $\left[C_t(\boldsymbol{p}_{t_0}, \boldsymbol{Q}_{t_0})\right]$. In other words, the complex quantity $C_t(\boldsymbol{p}_{t_0}, \boldsymbol{Q}_{t_0})$ is calculated at each time-step and its phase is obtained. In this way, we can approximate the product of the two pre-exponential factors as follows

$$C^*_{t_2}(\boldsymbol{p}_{t_1}, \boldsymbol{Q}_{t_1}) C_{t_2}(\boldsymbol{p}'_{t_1}, \boldsymbol{Q}'_{t_1}) \approx e^{i[\phi'(t_2)-\phi(t_2)]/\hbar} \left\{ e^{i[\phi'(t_1)-\phi(t_1)]/\hbar} \right\}^* . \tag{14}$$

The expression for the TA semiclassical absorption lineshape reads now as

$$\begin{aligned} \sigma(\omega, T) = & \iint \frac{d\boldsymbol{p}_0 d\boldsymbol{Q}_0}{(2\pi\hbar)^{N_\nu}} \iint \frac{d\boldsymbol{p}'_0 d\boldsymbol{Q}'_0}{(2\pi\hbar)^{N_\nu}} \frac{Re}{\pi T_s} \int_0^{T_s} dt_1 \int_{t_1}^{\infty} dt_2 \\ & \times e^{i\left[S_{t_2}(\boldsymbol{p}'_0, \boldsymbol{Q}'_0) - S_{t_2}(\boldsymbol{p}_0, \boldsymbol{Q}_0) - \hbar\omega t_2 + \phi'(t_2) - \phi(t_2)\right]/\hbar} \langle \boldsymbol{p}_{t_2} \boldsymbol{Q}_{t_2} | \hat{\mu} \hat{B}(\beta/2) | \boldsymbol{p}'_{t_2} \boldsymbol{Q}'_{t_2} \rangle \\ & \times \left\{ e^{i\left[S_{t_1}(\boldsymbol{p}'_0, \boldsymbol{Q}'_0) - S_{t_1}(\boldsymbol{p}_0, \boldsymbol{Q}_0) - \hbar\omega t_1 + \phi'(t_1) - \phi(t_1)\right]/\hbar} \langle \boldsymbol{p}_{t_1} \boldsymbol{Q}_{t_1} | \hat{\mu} \hat{B}(\beta/2) | \boldsymbol{p}'_{t_1} \boldsymbol{Q}'_{t_1} \rangle \right\}^* . \end{aligned} \tag{15}$$

Finally, setting the upper limit of the integral in t_2 equal to T_s, we easily get to the final expression

$$\begin{aligned} \sigma(\omega, T) = & \frac{(2\pi\hbar)^{-2N_\nu}}{2\pi T_s} \iint d\boldsymbol{p}_0 d\boldsymbol{Q}_0 \iint d\boldsymbol{p}'_0 d\boldsymbol{Q}'_0 \\ & \times \left| \int_0^{T_s} dt \, e^{i\left[S_t(\boldsymbol{p}'_0, \boldsymbol{Q}'_0) - S_t(\boldsymbol{p}_0, \boldsymbol{Q}_0) - \hbar\omega t + \phi'(t) - \phi(t)\right]/\hbar} \, \langle \boldsymbol{p}_t \boldsymbol{Q}_t | \hat{\mu} \hat{B}(\beta/2) | \boldsymbol{p}'_t \boldsymbol{Q}'_t \rangle \right|^2 . \end{aligned} \tag{16}$$

Therefore, according to Eq. 16, in order to calculate a semiclassical absorption lineshape, one first has to generate two sets of initial momenta and normal mode displacements, $(\boldsymbol{p}_0, \boldsymbol{Q}_0)$ and $(\boldsymbol{p}'_0, \boldsymbol{Q}'_0)$; then, pairs of trajectories starting from the two sets are run independently of one another under the classical Hamiltonian, for a total simulation time T_s. Finally, the squared modulus in Eq. 16 is evaluated for every pair of trajectories and summed together to give the global absorption lineshape. Starting from the expression of $\sigma(\omega, T)$, the semiclassical absorption spectrum $\alpha(\omega, T)$ can be readily recovered by means of Eq. 2a.

In this work, we investigate the expression of the semiclassical absorption spectrum for two limit cases: $T \to 0$ ($\beta \to +\infty$), and $T \to +\infty$ ($\beta \to 0$). At low temperatures, when $T \to 0$ ($\beta \to +\infty$), we can approximate the partition function as follows

$$\begin{aligned} Z &= \sum_n e^{-\beta E_n} = e^{-\beta E_0} + e^{-\beta E_1} + ... + e^{-\beta E_n} \\ &= e^{-\beta E_0}(1 + e^{-\beta(E_1 - E_0)} + ... + e^{-\beta(E_n - E_0)}) \approx e^{-\beta E_0}. \end{aligned} \tag{17}$$

As a consequence, the Boltzmann operator $\hat{B}(\beta)$ is represented as the projector on the vibrational ground state (the same clearly stands also for $\hat{B}(\beta/2)$)

$$\begin{aligned} \hat{B}(\beta) = \frac{e^{-\beta \hat{H}}}{Z} &\approx \sum_n e^{-\beta(E_n - E_0)} \left|\Psi_n\right\rangle \left\langle\Psi_n\right| \\ &= \left|\Psi_0\right\rangle \left\langle\Psi_0\right| + \sum_{n=1} e^{-\beta(E_n - E_0)} \left|\Psi_n\right\rangle \left\langle\Psi_n\right| \approx \left|\Psi_0\right\rangle \left\langle\Psi_0\right|, \end{aligned} \tag{18}$$

where we have expanded $e^{-\beta \hat{H}}$ on the complete orthonormal basis set given by the vibrational eigenstates. The bra-ket from Eq. 16 can then be rewritten as

$$\langle \boldsymbol{p}_t \boldsymbol{Q}_t | \hat{\mu} \hat{B}(\beta/2) | \boldsymbol{p}'_t \boldsymbol{Q}'_t \rangle = \langle \boldsymbol{p}_t \boldsymbol{Q}_t | \hat{\mu} | \Psi_0 \rangle \langle \Psi_0 | \boldsymbol{p}'_t \boldsymbol{Q}'_t \rangle . \tag{19}$$

At this point, we focus on the dipole moment operator. We employ the common linearization approximation to the molecular dipole moment

$$\boldsymbol{\mu}(\boldsymbol{q}) - \boldsymbol{\mu}(\boldsymbol{q}_{eq}) \simeq \sum_{j=1}^{N_\nu} \left.\frac{\partial \boldsymbol{\mu}}{\partial q_j}\right|_{\boldsymbol{q}_{eq}} (q_j - q_{eq,j}), \tag{20}$$

where the sum runs over the N_ν vibrational normal modes of the N-atom system ($3N - 5$ for linear molecules, $3N - 6$ otherwise). $\boldsymbol{\mu}(\boldsymbol{q})$ stands for the total dipole moment, meant as the sum of a nuclear contribution, $\boldsymbol{\mu}_N(\boldsymbol{R}) = \sum_i Z_i \boldsymbol{R}_i$, where Z_i are nuclear charges, and an electronic part, $\boldsymbol{\mu}_e(\boldsymbol{R}) = \int d\boldsymbol{r} |\varphi_0(\boldsymbol{r}; \boldsymbol{R})|^2 \boldsymbol{\mu}_e(\boldsymbol{r})$, with $\varphi_0(\boldsymbol{r}; \boldsymbol{R})$ being the adiabatic electronic ground state wavefunction for a given nuclear configuration. The introduction of the linearization approximation is particularly convenient since it allows one to avoid the direct computation of the electronic term $\boldsymbol{\mu}_e(\boldsymbol{R})$, which would require a challenging Monte Carlo estimate.[61]

In order to be able to calculate the bra-ket of Eq. 19 analytically, we approximate the vibrational ground state eigenfunction $|\Psi_0\rangle$ as the Hartree product of

one-dimensional ground state harmonic states

$$|\Psi_0\rangle \approx |\phi_0\rangle = |\phi_0^{(1)}, \phi_0^{(2)}, ..., \phi_0^{(N_\nu)}\rangle = |\phi_0^{(1)}\rangle \, ... \, |\phi_0^{(N_\nu)}\rangle \,, \tag{21}$$

where

$$\phi_0^{(j)}(Q_j) = \langle Q_j | \phi_0^{(j)} \rangle = \left(\frac{\omega_j}{\pi\hbar}\right)^{\frac{1}{4}} e^{-\frac{\omega_j}{2\hbar}Q_j^2}. \tag{22}$$

Hence, by inserting Eq. 20, 21 and 22 in Eq. 19, we get the following expression, employed in our calculations of low-temperature absorption spectra

$$\langle \boldsymbol{p}_t \boldsymbol{Q}_t | \hat{\mu} | \Psi_0 \rangle \, \langle \Psi_0 | \boldsymbol{p}_t' \boldsymbol{Q}_t' \rangle \approx \left[\sum_{j=1}^{N_\nu} \frac{\partial \boldsymbol{\mu}}{\partial q_j}\bigg|_{\boldsymbol{q}_{eq}} \left(\frac{Q_t^{(j)}}{2} - \frac{i}{2\omega_\alpha} p_t^{(j)} \right) \right] \langle \boldsymbol{p}_t \boldsymbol{Q}_t | \Psi_0 \rangle \, \langle \Psi_0 | \boldsymbol{p}_t' \boldsymbol{Q}_t' \rangle \,. \tag{23}$$

The overlap between the harmonic ground state and a coherent state can be calculated analytically, since

$$\langle \Psi_0 | \boldsymbol{p}_t \boldsymbol{Q}_t \rangle = \prod_{j=1}^{N_\nu} \langle \Psi_0^{(j)} | p_t^{(j)} Q_t^{(j)} \rangle \,, \tag{24}$$

with

$$\langle \Psi_0^{(j)} | p_t^{(j)} Q_t^{(j)} \rangle = \exp\left\{ -\frac{\omega_j}{4\hbar} \left[Q_t^{(j)} \right]^2 - \frac{1}{4\hbar\omega_j} \left[p_t^{(j)} \right]^2 - \frac{i}{2\hbar} p_t^{(j)} Q_t^{(j)} \right\}. \tag{25}$$

If we move to the high temperature limit ($T \to \infty$) the Boltzmann operator becomes equivalent to the identity operator

$$\hat{B}(\beta) = \frac{e^{-\beta\hat{H}}}{Z} = \frac{\sum_n e^{-\beta E_n} |\Psi_n\rangle \langle \Psi_n|}{\sum_n e^{-\beta E_n}} = \sum_n |\Psi_n\rangle \langle \Psi_n| = \hat{1}, \tag{26}$$

where we have used the fact that $e^{-\beta E_n} \to 1 \; \forall n$ (since $\beta \to 0$) and the complete basis set given by the vibrational eigenstates $|\Psi_n\rangle$.

Therefore, the bra-ket from the final expression of the vibrational lineshape (see Eq. 16) reduces, in the high temperature limit, to $\langle \boldsymbol{p}_t \boldsymbol{Q}_t | \hat{\mu} | \boldsymbol{p}_t' \boldsymbol{Q}_t' \rangle$, which can be computed by means of Eq. 20

$$\langle \boldsymbol{p}_t \boldsymbol{Q}_t | \hat{\mu} | \boldsymbol{p}_t' \boldsymbol{Q}_t' \rangle \approx \left[\sum_{j=1}^{N_\nu} \frac{\partial \boldsymbol{\mu}}{\partial q_j}\bigg|_{\boldsymbol{q}_{eq}} \left(\frac{Q_t^{(j)} + Q_t'^{(j)}}{2} - \frac{i}{\omega_j} \frac{p_t^{(j)} - p_t'^{(j)}}{2} \right) \right] \langle \boldsymbol{p}_t \boldsymbol{Q}_t | \boldsymbol{p}_t' \boldsymbol{Q}_t' \rangle \,. \tag{27}$$

The coherent state overlap in Eq. 27 can be evaluated analytically

$$\langle \boldsymbol{p}_t \boldsymbol{Q}_t | \boldsymbol{p}_t' \boldsymbol{Q}_t' \rangle = \prod_{j=1}^{N_\nu} \langle p_t^{(j)} Q_t^{(j)} | p_t'^{(j)} Q_t'^{(j)} \rangle \,, \tag{28}$$

with

$$\langle p_t^{(j)} Q_t^{(j)} | p_t'^{(j)} Q_t'^{(j)} \rangle = \exp\left[-\frac{\omega_j}{4\hbar} \left(Q_t^{(j)} - Q_t'^{(j)} \right)^2 - \frac{1}{4\hbar\omega_j} \left(p_t^{(j)} - p_t'^{(j)} \right)^2 \right] \times \exp\left[\frac{i}{2\hbar} \left(Q_t^{(j)} - Q_t'^{(j)} \right) \left(p_t^{(j)} + p_t'^{(j)} \right) \right]. \quad (29)$$

We point out that in the case of very high (namely infinite) temperature the evaluation of the absorption spectrum $\alpha(\omega, T)$ is meaningless because every eigenstate is equally populated, leading to a spectrum with null absorbance at all frequencies. Nevertheless, the absorption lineshape $\sigma(\omega, T \to \infty)$ still contains all the absorption frequencies of the system and we employ it to clarify some theoretical aspects of vibrational spectroscopy.

III. RESULTS

A. Morse oscillator

To test our approach we start from the study of a 1D Morse potential of the form

$$V(Q) = D_e \left[1 - e^{-\sqrt{\omega^2/2D_e} Q} \right]^2. \quad (30)$$

The harmonic frequency and the dissociation energy are set as $\omega = 4400$ cm^{-1} and $D_e = 38293$ cm^{-1}, respectively, mimicking the internal motion of an H_2 molecule. To select the initial conditions of the trajectories for the Monte Carlo phase-space integration (see Eq. 16), two Husimi distribution functions [70] are employed, both centered at the harmonic zero point energy (ZPE). 10000 pairs of trajectories are hence generated and evolved for 605 fs each (2500 time steps with $\Delta t = 10$ a.u.), with a rejection rate of 9.6%. For this analytical system both the IR spectrum at low temperature and the absorption lineshape at high T are calculated.

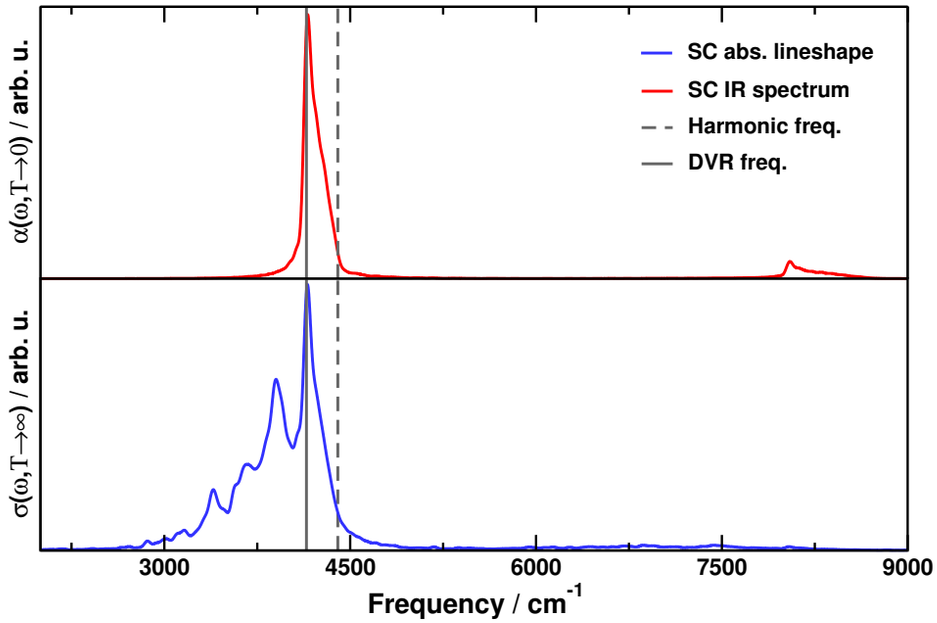

Figure 1: Semiclassical IR spectrum in the limit of low temperature (upper panel) and absorption lineshape at high temperature (bottom panel) for a 1D Morse oscillator. The dashed line corresponds to the harmonic estimate of the fundamental frequency of vibration. Quantum DVR estimate [61] of the same frequency is given by the vertical solid line.

The results reported in Figure 1 demonstrate an excellent agreement between our SC estimate and the one obtained by means of the Discrete Value Representation (DVR) technique, for both our simulations. In particular, the low temperature IR spectrum (panel (a) of Figure 1) shows an intense peak centered at 4157 cm^{-1}, corresponding to the fundamental $0 \rightarrow 1$ transition, and its weak quantum anharmonic overtone, centered at 8050 cm^{-1}. The high temperature absorption lineshape in the lower panel of Figure 1 presents, in addition to the main signal at 4155 cm^{-1}, a series of hot bands at increasingly lower frequencies. This happens because at high temperatures excited eigenstates get populated too, and transitions not involving the ground state are possible. The frequencies of these signals are compared to DVR analytical results in Table I, showing a very good level of agreement. An important aspect to point out is that the signal of the fundamental transition maintains (within expected numerical accuracy) the same frequency when switching from low to high temperature (4157 vs 4155 cm^{-1}). This evidence proves our method to

be temperature independent as far as frequency evaluation is concerned as any approach based on quantum mechanics is expected to be, given that temperature does not enter the Schroedinger equation (conversely absorption intensities are indeed temperature dependent).[71] As an aside, we notice that for this simple 1D system an exact DVR calculation of the intensity of hot bands is doable. We report it in the Supplementary Material file, where it is shown that, as predicted from the SC theory, agreement between SC and DVR calculations for hot bands improves as we move the center of the sampling of trajectory energies from the harmonic ZPE to values closer to the energy of the states involved in the hot band transitions.

Table I: Absorption frequencies in cm^{-1} for the indicated transitions ($i \to f$) of the 1D Morse oscillator.

$i \to f$	Semiclassical	DVR
$0 \to 1$	4155	4147.33
$1 \to 2$	3901	3894.92
$2 \to 3$	3669	3643.07
$3 \to 4$	3395	3391.95
$0 \to 2$	8050	8042.26
MAE	10	-

B. H_2O

Increasing the number of degrees of freedom, we apply our method to the non-rotating water molecule in vacuum. This system is characterized by $3N - 6 = 3$ normal modes of vibration, namely the bending mode (ν_b), the symmetric stretch (ν_{ss}), and the asymmetric stretch (ν_{as}). In our calculations we employ a pre-existing analytical potential energy surface (PES) based on a quartic force field.[72] As for the dipole derivatives at the equilibrium geometry appearing in Eq. 20, instead, we

employ the values employed in a previous work [62], in which the dipole derivatives were calculated by means of an analytical dipole moment surface.[73]

For the water molecule, we focus on the calculation of the semiclassical low-temperature IR spectrum. To this end, 10^5 pairs of trajectories are selected through two Husimi distribution functions centered at the harmonic ZPE, and evolved for 605 fs (2500 steps with $\Delta t = 10$ a.u.). The final rejection rate is 23.7%.

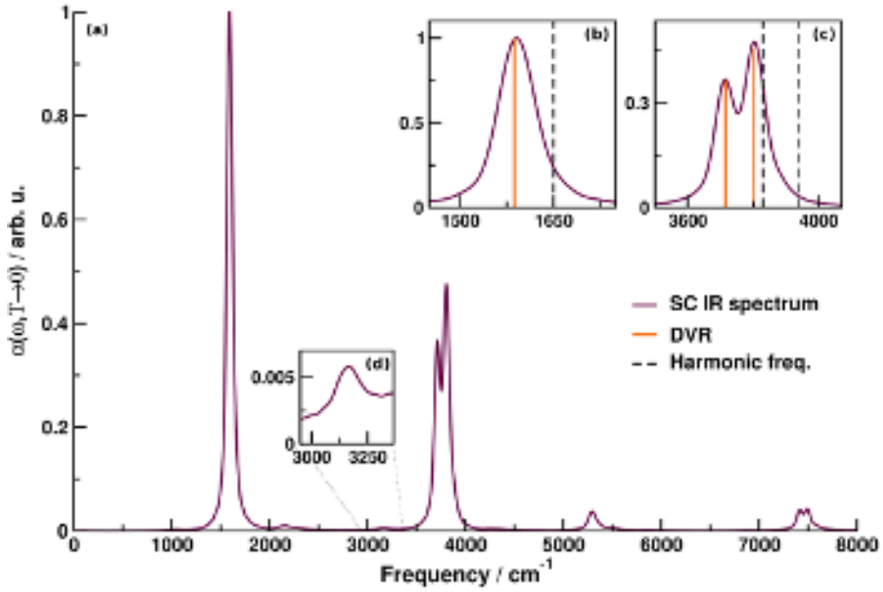

Figure 2: Panel (a): Semiclassical IR spectrum of the water molecule in vacuum in the low temperature limit. Panels (b) and (c): zoom on the bending signal, and the fundamental signals related to the symmetric and asymmetric stretches, respectively, with harmonic frequency estimates (dashed lines) and DVR frequency and intensity benchmarks [62] (full orange lines). Panel (d): zoom on the bending overtone.

Panel (a) of Figure 2 shows the absorption spectrum obtained from our calculation. It is made of several features, namely the fundamental peaks related to the bending mode and symmetric and asymmetric stretches, located at 1591, 3715 and 3804 cm^{-1} respectively, a combination band at 5294 cm^{-1}, due to the simultaneous excitation of the bending and one stretching mode, and the overtone signals, centered at 3166 cm^{-1} for the bending and at 7416 and 7490 cm^{-1} for the stretching modes. In panels (b) and (c) we report a zoom on the three fundamental tran-

sitions, to compare both their frequencies and intensities with the DVR reference values (taken from Ref 62).

The results show that our method is able to reproduce the DVR values with an excellent level of accuracy, considering both the frequencies, with a maximum deviation of 4 cm^{-1}, and the relative intensities of the peaks. Indeed, upon normalization of the spectral intensities to the peak of maximum intensity, i.e. the bending, we find that the intensities of the symmetric and asymmetric fundamental signals match the DVR reference ones with percentage errors of 1.2% and 4.0%, respectively. The slightly higher error involving the asymmetric stretch signal may be due to the fact that the two Husimi distribution functions employed to select the initial conditions of the trajectories are both centered at the harmonic zero point energy, hence further away in energy from the first excited state of this normal mode than they are for the symmetric stretch. Panel (d) of Figure 2 shows a zoom on the bending overtone, resonating at 3166 cm^{-1}. Its intensity can be compared to the one calculated by Micciarelli *et al.* by means of a more elaborated semiclassical approach based on the preliminar computation of semiclassical wavefunctions.[62] A good level of agreement is found, since in both cases the signal intensity is in the order of magnitude of 10^{-3} : 1 relative to the fundamental transition associated to the bending absorption peak.

By carefully inspecting the IR spectrum in panel (a) of Figure 2, one finds out that it also presents a signal at 2157 cm^{-1}, whose frequency does not correspond to any fundamental, combination or overtone band of the system. In fact, its frequency can be identified as the difference between the symmetric stretch and the bending frequencies. This signal, however, does not appear in the experimental IR spectra, since the (1,0,0) excited state is not sizeably populated for the isolated water molecule at low (and also room!) temperature. Hence, to investigate the origin of this signal we perform an additional set of calculations with increasing simulation time. The results are reported in Figure 3, and show how the relative intensity of the peak tends to decrease by evolving longer trajectories, proving that its presence is not related to any actual physical effect of the system, but it is simply a numerical artifact due to the finite duration of our simulations. More on this will be discussed

in the final Summary, Conclusions, and Perspectives Section.

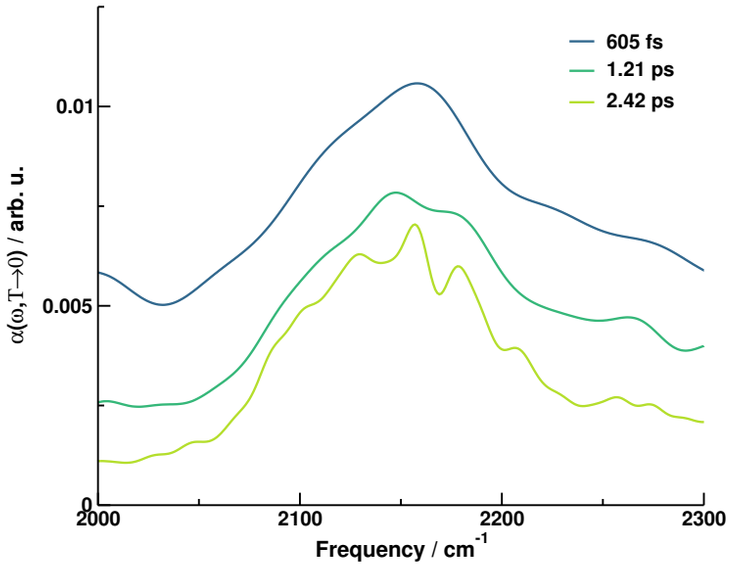

Figure 3: Zoom on the peak centered at 2147 - 2158 cm^{-1} from the semiclassical IR spectra of the non-rotating water molecule in vacuum, obtained by evolving 10^4 couples of trajectories with increasing time-length (2500, 5000 and 10000 au). The corresponding rejection rates are 24%, 49% and 74%, respectively. The spectra are shown upon normalization to the maximum of the bending absorption.

C. CO_2

The last application we propose is the non-rotating CO_2 molecule in vacuum, a linear molecule characterized by $3N - 5 = 4$ vibrational degrees of freedom. They are a symmetric stretching mode (ν_{ss}), two degenerate bending modes (ν_b and $\bar{\nu}_b$) and an asymmetric stretching mode (ν_{as}). Also in this case, a pre-existing *ab-initio* quartic PES[74] is employed in our calculations. It is common to label quantum states of the CO_2 molecule by means of a triplet of quantum numbers (n_{ss}, n_b, n_{as}) referred to symmetric stretch, bending, and asymmetric stretch, respectively.

We do not have an analytical dipole moment surface available for this system, so we evaluate the dipole derivatives of Eq. 20 by performing a DFT B3LYP-D3/aug-cc-pvdz geometry optimization and frequency calculation on the NWChem *ab-initio* software,[75] starting from the equilibrium geometry of the PES as an initial guess.

We then calculate the low-temperature (rigorously 0K) semiclassical IR spectrum by evolving 10^4 pairs of trajectories 1.2 ps long (5000 steps with $\Delta t = 10$ a.u.) on the PES, with a final rejection rate of 4.5%. Also in this case, we select the initial conditions of the dynamics by means of two Husimi distribution functions centered at the harmonic ZPE. For the purpose of making a direct comparison we also calculate the vibrational power spectrum of this molecule, by means of a TA-SCIVR approach based on the same computational setup (PES, number, initial conditions, and time length of the trajectories). The results of the two calculations are reported in Figure 4, where the reference QM frequencies, which we label as "exact QM frequencies", were calculated through a vibrational full configuration interaction method in a finite basis representation (see Ref. 76).

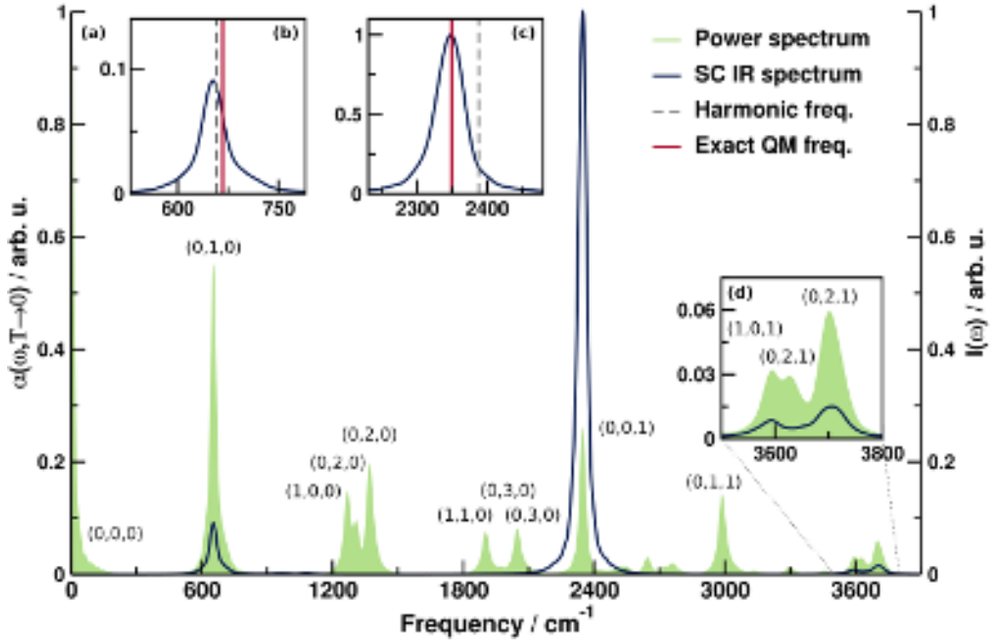

Figure 4: Panels (a) and (d): Semiclassical low-temperature IR spectrum (full blue line) and vibrational power spectrum (green area) for the CO_2 molecule in vacuum. ZPE signal in the power spectrum has been shifted to zero for direct comparison. The left y-axis refers to the IR spectrum, while the right one to the power spectrum. Panels (b) and (c): zoom on the fundamental IR bands of the degenerate bending modes and the asymmetric stretch, respectively, together with the harmonic (dashed line) and the reference QM (full red line) frequency values. [76]

By comparing the signals of the two spectra, we demonstrate that the semi-classical IR spectrum is able to select only the transitions that are allowed by the symmetry-based quantum selection rules, differently from the power spectrum, which, by definition, determines all energy levels and, therefore, can be used to show all the possible transitions from the ground vibrational state to the excited ones. The linear CO_2 molecule belongs to the $D_{\infty h}$ point group, hence the only IR active (combinations of) normal modes are those characterized by the Π_u or Σ_u^+ symmetry species. In particular, we point out that motions symmetrical with respect to the inversion center of the molecule (those indicated by the g subscript) are IR inactive.

The first signal found in the power spectrum after the ZPE is the fundamental transition of the degenerate bending modes, labeled as (0,1,0). At the same frequency, 653 cm^{-1}, a peak in the IR spectrum is also present, and this is justified by the fact that this motion possesses a Π_u symmetry. Then, in the region between 1200 and 1400 cm^{-1} the power spectrum shows three bands: the first one, centered at 1268 cm^{-1}, is assigned to the fundamental of the symmetric stretch mode (1,0,0); its symmetry species is Σ_g^+ and, correctly, no IR signal is found at that frequency. The two peaks at 1308 and 1370 cm^{-1}, instead, are both labeled as bending overtones (0,2,0), since they arise from the direct product of the two Π_u symmetry species. These are two signals slightly split in frequency due to different vibrational angular momentum, with symmetry Σ_g^+ and Δ_g, and therefore both IR inactive. Between 1900 and 2050 cm^{-1} the power spectrum shows the (1,1,0) combination band and two split signals of the triple bending overtone, (0,3,0). According to the selection rules, the former and one of the latter signals are IR active, being characterized by the Π_u symmetry . However, given the nature of the two signals, it is reasonable to assume that their intensity is extremely low and cannot clearly emerge from the baseline of the IR spectrum. At 2348 cm^{-1} the fundamental transition of the asymmetric stretch (0,0,1) appears both in the power and in the infrared spectra, as expected given the Σ_u^+ symmetry of this normal mode. The combination band given by the simultaneous absorption of the bending and the asymmetric stretch modes (0,1,1), centered at 2988 cm^{-1} in the power spectrum, is IR inactive, given its Π_g symmetry, and indeed does not appear in the IR spectrum. Finally, as shown

in panel (d) of Figure 4, three peaks are observed in the power spectrum between 3500 and 3800 cm^{-1}. The first one is assigned to the symmetric and asymmetric stretch mode combination band (1,0,1) of Σ_u^+ symmetry, and therefore it is also visible in our IR spectrum. The other two signals are due to the (0,2,1) absorption, which, analogously to the (0,2,0) and (0,3,0) cases reviewed above, is split due to vibrational angular momentum reasons. The first one of these, with symmetry Δ_u, is IR inactive, while the second one, of symmetry Σ_u^+, is IR active and resonates at a slightly higher frequency. This explains why in the IR spectrum two signals are present in this region, while three signals can be observed in the power spectrum. A Table in the Supplementary Material collects all mentioned data about symmetries of CO_2 vibrational motions.

Therefore, at the end of this analysis, we are able to verify that the method we propose for the calculation of semiclassical IR spectra is able to fully abide by the quantum selection rules, not showing those transitions which are inactive according to their symmetry. On the other hand, as shown above, not all the IR active absorptions appear as visible signals in the spectrum, but this can be explained by considering that the intensity of any IR band is also related to the magnitude of the corresponding transition dipole moment, which, if low, can quench the intensity of the signal.

Finally, as far as the accuracy of our method is concerned, we can observe by looking at panels (b) and (c) in Figure 4 that the frequencies of the bending and the asymmetric stretch fundamentals are reasonably close to the exact values reported, especially for the stretching mode, while for the bending a discrepancy of just 14 cm^{-1} is found. As for the intensities of our absorption peaks, not having any reference quantum mechanical calculation available, we report in Figure 5 a comparison between our calculated IR spectrum and the experimental ro-vibrational spectrum of carbon dioxide in the gas phase. Although the comparison cannot be totally on the same level, since the peaks of the experimental spectrum correspond to ro-vibrational transitions instead of the pure vibrational transitions simulated by us, a good level of agreement is observed both for frequencies and the relative intensity ratios.

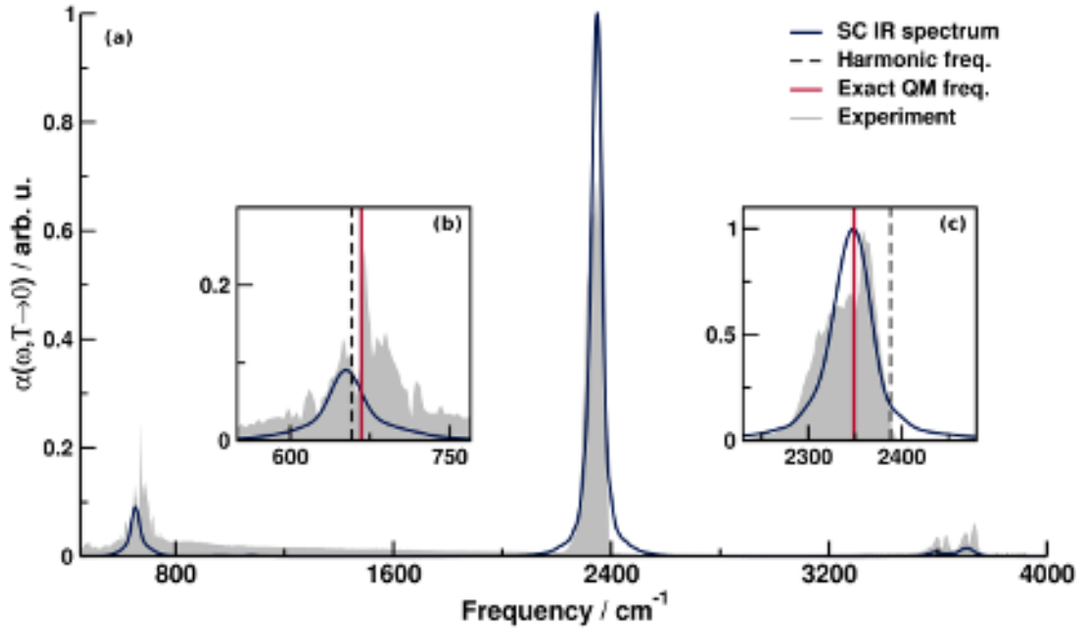

Figure 5: Panel (a): Semiclassical low-temperature IR spectrum (full blue line) and experimental ro-vibrational spectrum (gray area) of the CO_2 molecule. Panels (b) and (c): zoom on the bending and asymmetric stretch modes fundamental transitions, respectively, reported with the corresponding harmonic (dashed line) and exact (full red line) frequency values.

IV. SUMMARY, CONCLUSIONS, AND PERSPECTIVES

In this paper, we have demonstrated that the time average semiclassical technique, first introduced by Kaledin and Miller to deal with power spectra, can actually be employed to get a practical expression for semiclassical IR spectra. The main difference with the power spectra expression lies in the necessity to run trajectories in pairs for the IR spectrum (due to a double phase space integration) instead of the single trajectories used for the power spectrum (due to a single phase space integration). This keeps the computational overhead still affordable while allowing to obtain accurate spectra in both intensities and frequencies. We were able to study model and molecular systems of increasing dimensionality (single Morse oscillator, H_2O molecule, and CO_2 molecule) describing quantitatively the relative intensities of absorption peaks and taking into account correctly transition rules

related to molecular symmetry. On this regard, we point out that our method is totally general and does not rely on symmetry properties. In other words, we found out the expected results, which were predictable on the basis of symmetry reasoning, without enforcing symmetry in our calculations.

The application to the water molecule has allowed us to analyze an unexpected signal at around 2150 cm^{-1}. In liquid water that is the region of the libration-bending combination band. Clearly, such a band cannot be present in the isolated water molecule spectrum, since there are no librations in the isolated molecule. We have considered several possible reasons to explain the presence of this signal, ranging from the necessity to reach better convergence of our calculations to the separable approximation employed for the SC prefactor, from the presence of a small angular momentum in the trajectories leading to the observed signal to the necessity to employ longer trajectories to deal with the Fourier transform included in the time average. While the first three hypotheses were excluded upon calculations not reported here, the latter has been found responsible for the observed peak. This has been reported in Fig. 3. An interesting point about this investigation is that the signal at about 2150 cm^{-1} can be interpreted as related to the frequency difference between a stretch and the bending modes. As demonstrated in the paper, this feature is disappearing as the simulation time is increased and a more accurate evaluation of the Fourier transform is obtained. However, as the simulation time increases, the SC propagator is known to lose its quantum character moving towards a (quasi-)classical description.[77] This explains why we could not eliminate completely the 2150 cm^{-1} peak from our spectrum: indeed, classical simulations can be theoretically expected to give signals at frequency differences,[78] and by increasing the simulation time our SC simulation is moving towards a classical description. Given the weak intensity of such signals and the fact we can easily locate them in frequency, the inability to completely eliminate them from our IR spectra does not jeopardize the global interpretation of our spectra. The topic of spectral differences between quantum and classical trajectory-based approaches is a very interesting one, allowing one to characterize the quantum or classical character of different techniques, and therefore it will be the target of one of our future papers.

We presented our new approach in the two limits of high (infinite) and low (0K) temperature. In particular, the 0K spectrum is usually a realistic representation of molecular vibrational spectra since low energy levels are well separated and population distribution among energy levels at room temperature is basically equal to that at 0K (i.e. only the ground state is populated). However, this approximation is less and less accurate as the complexity and dimensionality of the molecular system increases since energy levels get closer to each other.[79] A future development of our approach will consist in considering finite temperature effects. A nice way to do this is represented by thermo-field dynamics. By using thermo-field dynamics one can incorporate finite-temperature effects in the calculation at the cost of doubling the number of degrees of freedom. The computational cost of calculation is independent of temperature, and the technique has been adopted together with SC thawed Gaussian approaches.[80, 81] Another possible approach to take into account finite temperature effects consists in including (in an approximate way) more terms in the expansion of the Boltzmann operator on the vibrational eigenstate basis set. The final SC expression will be a little more elaborated, but computational costs will be similar to a 0K calculation.

Finally, it must be pointed out that this new approach to IR spectroscopy has the advantage of preserving the theoretical framework of SC power spectra. The natural consequence of this fact is that the several techniques developed for calculations of power spectra can be adopted for IR spectroscopy, leading to an improved and complete semiclassical description of the vibrational spectroscopy of large and complex molecular systems. SC power spectra have already been demonstrated as a valuable tool to solve open experimental topics involving quantum effects in complex systems, based on frequency evaluation only.[71, 82] The tool presented in this paper will allow to look also at absorption intensities, thus much increasing the effectiveness of a semiclassical study.

V. SUPPLEMENTARY MATERIAL

Details on an additional simulation of the semiclassical absorption lineshape of the 1D Morse potential performed at high temperature ($T \to \infty$) with an extended

sampling can be found in the Supplementary Material, together with a comparison between our calculated absorption frequencies of the water molecule and corresponding reference values, and a table containing detailed data about symmetries of CO_2 vibrational motions.

Acknowledgments

R.C. and M.C. thank Università degli Studi di Milano for funding under project PSR2022_DIP_005_PI_RCONT. C.A. thanks Università degli Studi di Milano for funding under project PSR2022_DIP_005_PI_CAIET. M.C. and C.L. acknowledge financial support from the European Research Council (grant agreement no. 101081361 - SEMISOFT - ERC-2022- POC2 under the Horizon Europe research and innovation programme). R.C. acknowledges the CINECA award IsCa7_CombH2O, under the ISCRA initiative, for the availability of high-performance computing resources and support.

Bibliography

[1] F. t. Braak, H. Elferink, K. J. Houthuijs, J. Oomens, J. Martens, and T. J. Boltje, Acc. Chem. Res. **55**, 1669 (2022).

[2] M. C. Celina, N. H. Giron, and M. R. Rojo, Polymer **53**, 4461 (2012).

[3] E. R. K. Neo, Z. Yeo, J. S. C. Low, V. Goodship, and K. Debattista, Resour. Conserv. Recycl. **180**, 106217 (2022).

[4] J. A. Boatz and M. S. Gordon, J. Phys. Chem. **93**, 1819 (1989).

[5] M. Wehrle, M. Sulc, and J. Vanicek, J. Chem. Phys. **140**, 244114 (2014).

[6] J. S. Bader and B. J. Berne, J. Chem. Phys. **100**, 8359 (1994).

[7] D. Moscato, G. Mandelli, M. Bondanza, F. Lipparini, R. Conte, B. Mennucci, and M. Ceotto, J. Am. Chem. Soc. **146**, 8179 (2024).

[8] D. A. McQuarrie, *Statistical Mechanics* (Harper-Collins, 1976).

[9] J. J. Goings, P. J. Lestrange, and X. Li, Wiley Interdisciplinary Reviews: Comput. Mol. Sci. **8**, e1341 (2018).

[10] T. Mathea and G. Rauhut, J. Chem. Phys. **152**, 194112 (2020).

[11] H. Liu, Y. Wang, and J. M. Bowman, J. Chem. Phys. **142**, 194502 (2015).

[12] C. Qu and J. M. Bowman, Phys. Chem. Chem. Phys. **21**, 3397 (2019).

[13] V. Barone, J. Bloino, C. A. Guido, and F. Lipparini, Chem. Phys. Lett. **496**, 157 (2010).

[14] M. Biczysko, J. Bloino, I. Carnimeo, P. Panek, and V. Barone, J. Mol. Struct. **1009**, 74 (2012).

[15] O. Vendrell, F. Gatti, and H.-D. Meyer, J. Chem. Phys. **127**, 184303 (2007).

[16] M. Bonfanti, J. Petersen, P. Eisenbrandt, I. Burghardt, and E. Pollak, J. Chem. Theory Comput. **14**, 5310 (2018).

[17] S. Habershon, G. S. Fanourgakis, and D. E. Manolopoulos, J. Chem. Phys. **129** (2008).

[18] T. Fletcher, A. Zhu, J. E. Lawrence, and D. E. Manolopoulos, J. Chem. Phys. **155** (2021).

[19] W. H. Miller and T. F. George, J. Chem. Phys. **56**, 5637 (1972).

[20] E. J. Heller, Acc. Chem. Res. **14**, 368 (1981).

[21] W. H. Miller, Proc. Natl. Acad. Sci. USA **102**, 6660 (2005).

[22] R. Hernandez and W. H. Miller, Chem. Phys. Lett. **214**, 129 (1993).

[23] J. O. Richardson, J. Chem. Phys. **144** (2016), 10.1063/1.4943866, 114106, https://pubs.aip.org/aip/jcp/article-pdf/doi/10.1063/1.4943866/13615318/114106_1_online.pdf .

[24] C. Aieta and M. Ceotto, J. Chem. Phys. **146**, 214115 (2017).

[25] T. L. Nguyen, J. R. Barker, and J. F. Stanton, in *Adv. Atmosph. Chem.* (World Scientific, 2017) pp. 403–492.

[26] J. O. Richardson, Int. Rev. Phys. Chem. **37**, 171 (2018), https://doi.org/10.1080/0144235X.2018.1472353 .

[27] C. Aieta, F. Gabas, and M. Ceotto, J. Chem. Theory Comput. **15**, 2142 (2019).

[28] G. Mandelli, L. Corneo, and C. Aieta, J. Phys. Chem. Lett. **14**, 9996 (2023).

[29] C. Aieta, M. Micciarelli, G. Bertaina, and M. Ceotto, Nat. Comm. **11**, 4384 (2020).

[30] C. Aieta, G. Bertaina, M. Micciarelli, and M. Ceotto, J. Chem. Phys. **153**, 214117 (2020).

[31] J. Ankerhold, F. Grossmann, and D. J. Tannor, Phys. Chem. Chem. Phys. **1**, 1333 (1999).

[32] W. Koch, F. Großmann, J. T. Stockburger, and J. Ankerhold, Phys. Rev. Lett. **100**, 230402 (2008).

[33] R. Conte and E. Pollak, J. Chem. Phys. **136**, 094101 (2012).

[34] F. Grossmann, Comments At. Mol. Phys. **34**, 141 (1999).

[35] M. Buchholz, F. Grossmann, and M. Ceotto, J. Chem. Phys. **147**, 164110 (2017).

[36] M. Buchholz, F. Grossmann, and M. Ceotto, J. Chem. Phys. **144**, 094102 (2016).

[37] M. S. Church and N. Ananth, J. Chem. Phys. **151**, 134109 (2019).

[38] M. S. Church, S. V. Antipov, and N. Ananth, J. Chem. Phys. **146**, 234104 (2017).

[39] S. V. Antipov, Z. Ye, and N. Ananth, J. Chem. Phys. **142**, 184102 (2015).

[40] D. Huber and E. J. Heller, J. Chem. Phys. **87**, 5302 (1987).

[41] K. G. Kay, J. Chem. Phys. **101**, 2250 (1994).

[42] F. Grossmann and A. L. Xavier, Phys. Lett. A **243**, 243 (1998).

[43] W. H. Miller, J. Phys. Chem. A **105**, 2942 (2001).

[44] W. H. Miller, Mol. Phys. **100**, 397 (2002).

[45] D. V. Shalashilin and M. S. Child, Chem. Phys. **304**, 103 (2004).

[46] E. Pollak, "The Semiclassical Initial Value Series Representation of the Quantum Propagator," in *Quantum Dynamics of Complex Molecular Systems* (Springer Berlin Heidelberg, Berlin, Heidelberg, 2007) pp. 259–271.

[47] A. L. Kaledin and W. H. Miller, J. Chem. Phys. **118**, 7174 (2003).

[48] A. L. Kaledin and W. H. Miller, J. Chem. Phys. **119**, 3078 (2003).

[49] M. Ceotto, S. Atahan, G. F. Tantardini, and A. Aspuru-Guzik, J. Chem. Phys. **130**, 234113 (2009).

[50] M. Ceotto, G. Di Liberto, and R. Conte, Phys. Rev. Lett. **119**, 010401 (2017).

[51] A. Rognoni, R. Conte, and M. Ceotto, Chem. Sci. **12**, 2060 (2021).

[52] A. Rognoni, R. Conte, and M. Ceotto, J. Chem. Phys. **154**, 094106 (2021).

[53] L. Mino, M. Cazzaniga, F. Moriggi, and M. Ceotto, J. Phys. Chem. C **127**, 437 (2023).

[54] R. Conte, L. Parma, C. Aieta, A. Rognoni, and M. Ceotto, J. Chem. Phys. **151**, 214107 (2019).

[55] G. Botti, M. Ceotto, and R. Conte, J. Chem. Phys. **155**, 234102 (2021).

[56] G. Botti, C. Aieta, and R. Conte, J. Chem. Phys. **156**, 164303 (2022).

[57] J.-X. Zeng, S. Yang, Y.-C. Zhu, W. Fang, L. Jiang, E.-G. Wang, D. H. Zhang, and X.-Z. Li, J. Phys. Chem. A **127**, 2902 (2023).

[58] M. Wehrle, S. Oberli, and J. Vaníček, J. Phys. Chem. A **119**, 5685 (2015).

[59] A. Patoz, T. Begusic, and J. Vanicek, J. Phys. Chem. Lett. **9**, 2367 (2018).

[60] R. Moghaddasi Fereidani and J. Vanicek, J. Chem. Phys. **160**, 044113 (2024).

[61] M. Micciarelli, R. Conte, J. Suarez, and M. Ceotto, J. Chem. Phys. **149**, 064115 (2018).

[62] M. Micciarelli, F. Gabas, R. Conte, and M. Ceotto, J. Chem. Phys. **150**, 184113 (2019).

[63] X. Sun, H. Wang, and W. H. Miller, J. Chem. Phys. **109**, 4190 (1998).

[64] M. F. Herman and E. Kluk, Chem. Phys. **91**, 27 (1984).

[65] K. G. Kay, Chem. Phys. **322**, 3 (2006).

[66] E. J. Heller, J. Chem. Phys. **75**, 2923 (1981).

[67] W. H. Miller and T. F. George, J. Chem. Phys. **56**, 5637 (1972).

[68] L. Bonnet, J. Chem. Phys. **153** (2020).

[69] L. Bonnet, J. Chem. Phys. **158** (2023).

[70] K. Husimi, Proc. Phys. Math. Soc. Jpn. 3rd Series **22**, 264 (1940).

[71] R. Conte, C. Aieta, G. Botti, M. Cazzaniga, M. Gandolfi, C. Lanzi, D. Moscato, and M. Ceotto, Theor. Chem. Acc. (2023), 10.1007/s00214-023-02993-y.

[72] S. Dressler and W. Thiel, Chem. Phys. Lett. **273**, 71 (1997).

[73] L. Lodi, J. Tennyson, and O. L. Polyansky, J. Chem. Phys. **135**, 034113 (2011).

[74] J. Martin, P. R. Taylor, and T. J. Lee, Chem. Phys. Lett. **205**, 535 (1993).

[75] M. Valiev, E. Bylaska, N. Govind, K. Kowalski, T. Straatsma, H. Van Dam, D. Wang, J. Nieplocha, E. Apra, T. Windus, and W. de Jong, Comput. Phys. Commun. **181**, 1477 (2010).

[76] J. Vázquez, M. E. Harding, J. F. Stanton, and J. Gauss, J. Chem. Theory Comput. **7**, 1428 (2011).

[77] S. Zhang and E. Pollak, J. Chem. Phys. **119**, 11058 (2003).

[78] L. D. Landau and E. M. Lifshitz, *Mechanics* (Elsevier, 1982).

[79] C. Aieta, F. Gabas, and M. Ceotto, J. Phys. Chem. A **120**, 4853 (2016).

[80] C. S. Reddy and M. D. Prasad, J. Phys. Chem. A **120**, 2583 (2016).

[81] T. Begušić and J. Vaníček, J. Chem. Phys. **153** (2020).

[82] F. Gabas, G. Di Liberto, R. Conte, and M. Ceotto, Chem. Sci. **9**, 7894 (2018).